AMERICAN SOCIETY FOR MICROBIOLOGY | Journal of Virology®

VIRUS-CELL INTERACTIONS

SARS-CoV-2 and Three Related Coronaviruses Utilize Multiple ACE2 Orthologs and Are Potently Blocked by an Improved ACE2-Ig

Yujun Li,[a] Haimin Wang,[a] Xiaojuan Tang,[a] Shisong Fang,[c] Danting Ma,[a] Chengzhi Du,[a,b] Yifei Wang,[a] Hong Pan,[a,b] Weitong Yao,[a,b] Renli Zhang,[c] Xuan Zou,[c] Jie Zheng,[d] Liangde Xu,[e] Michael Farzan,[f] Guocai Zhong[a,b]

[a]Institute of Chemical Biology, Shenzhen Bay Laboratory, Shenzhen, China
[b]School of Chemical Biology and Biotechnology, Peking University Shenzhen Graduate School, Shenzhen, China
[c]Shenzhen Center for Disease Control and Prevention, Shenzhen, China
[d]Shanghai Institute of Materia Medica, Chinese Academy of Sciences, Shanghai, China
[e]School of Biomedical Engineering and Eye Hospital, Wenzhou Medical University, Wenzhou, China
[f]Department of Immunology and Microbiology, The Scripps Research Institute, Jupiter, Florida, USA

Yujun Li, Haimin Wang, Xiaojuan Tang, and Shisong Fang contributed equally to this article. Author order was determined by minor contribution difference.

ABSTRACT The ongoing coronavirus disease 2019 (COVID-19) pandemic has caused >20 million infections and >750,000 deaths. Severe acute respiratory syndrome coronavirus 2 (SARS-CoV-2), the etiological agent of COVID-19, has been found closely related to the bat coronavirus strain RaTG13 (Bat-CoV RaTG13) and a recently identified pangolin coronavirus (Pangolin-CoV-2020). Here, we first investigated the ability of SARS-CoV-2 and three related coronaviruses to utilize animal orthologs of angiotensin-converting enzyme 2 (ACE2) for cell entry. We found that ACE2 orthologs of a wide range of domestic and wild mammals, including camels, cattle, horses, goats, sheep, cats, rabbits, and pangolins, were able to support cell entry of SARS-CoV-2, suggesting that these species might be able to harbor and spread this virus. In addition, the pangolin and bat coronaviruses, Pangolin-CoV-2020 and Bat-CoV RaTG13, were also found able to utilize human ACE2 and a number of animal-ACE2 orthologs for cell entry, indicating risks of spillover of these viruses into humans in the future. We then developed potently anticoronavirus ACE2-Ig proteins that are broadly effective against the four distinct coronaviruses. In particular, through truncating ACE2 at its residue 740 but not 615, introducing a D30E mutation, and adopting an antibody-like tetrameric-ACE2 configuration, we generated an ACE2-Ig variant that neutralizes SARS-CoV-2 at picomolar range. These data demonstrate that the improved ACE2-Ig variants developed in this study could potentially be developed to protect from SARS-CoV-2 and some other SARS-like viruses that might spillover into humans in the future.

IMPORTANCE The severe acute respiratory syndrome coronavirus 2 (SARS-CoV-2) is the etiological agent of the currently uncontrolled coronavirus disease 2019 (COVID-19) pandemic. It is important to study the host range of SARS-CoV-2, because some domestic species might harbor the virus and transmit it back to humans. In addition, insight into the ability of SARS-CoV-2 and SARS-like viruses to utilize animal orthologs of the SARS-CoV-2 receptor ACE2 might provide structural insight into improving ACE2-based viral entry inhibitors. In this study, we found that ACE2 orthologs of a wide range of domestic and wild animals can support cell entry of SARS-CoV-2 and three related coronaviruses, providing insights into identifying animal hosts of these viruses. We also developed recombinant ACE2-Ig proteins that are able to potently block these viral infections, providing a promising approach to developing antiviral proteins broadly effective against these distinct coronaviruses.

Citation Li Y, Wang H, Tang X, Fang S, Ma D, Du C, Wang Y, Pan H, Yao W, Zhang R, Zou X, Zheng J, Xu L, Farzan M, Zhong G. 2020. SARS-CoV-2 and three related coronaviruses utilize multiple ACE2 orthologs and are potently blocked by an improved ACE2-Ig. J Virol 94:e01283-20. https://doi.org/10.1128/JVI.01283-20.

Editor Tom Gallagher, Loyola University Chicago

Address correspondence to Guocai Zhong, zhonggc@szbl.ac.cn.

Received 24 June 2020
Accepted 20 August 2020
Accepted manuscript posted online 26 August 2020
Published 27 October 2020

KEYWORDS ACE2, ACE2-Ig, SARS-CoV-2, entry inhibitor, host range

Two subgroups of coronaviruses, including alphacoronaviruses (e.g., swine acute diarrhea syndrome coronavirus [SADS-CoV]) and betacoronaviruses (e.g., severe acute respiratory syndrome coronavirus [SARS-CoV]), infect mammals and have broad host ranges spanning bats, rodents, domestic animals, and humans (1–7). Bats are considered to be the natural reservoir hosts for a number of pathogenic human coronaviruses, including SARS-CoV, Middle East respiratory syndrome coronavirus (MERS-CoV), HCoV-NL63, and HCoV-229E (6, 8). The severe acute respiratory syndrome coronavirus 2 (SARS-CoV-2), the etiological agent of coronavirus disease 2019 (COVID-19) (8–10), shares 79.5% genome sequence identity to SARS-CoV and 96.2% genome sequence identity to Bat-CoV RaTG13, a coronavirus detected in bat species *Rhinolophus affinis*, indicating that bats are also likely a reservoir host for SARS-CoV-2 (8–10). Multiple SARS-CoV-2-related coronaviruses with 85.5 to 92.4% genome sequence similarity to SARS-CoV-2 have been identified in Malayan pangolins (*Manis javanica*) recently (11–13). Two of these pangolin coronaviruses, called Pangolin-CoV-2020 (11) and GD Pangolin CoV (12), have 90.23 and 92.4% genome sequence similarity to SARS-CoV-2, respectively, and have only one amino acid different from SARS-CoV-2 within the spike protein receptor binding motif (RBM) region. Based on these findings, pangolins have been proposed as an intermediate host or another natural host of SARS-CoV-2 (11–13). Domestic animals have been shown to play key roles as intermediate hosts, such as camels for MERS-CoV and camelids for HCoV-229E, to transmit pathogenic coronaviruses from bats to humans (6). It is unknown whether domestic animals also play roles on SARS-CoV-2 transmission.

As of 15 August 2020, the ongoing COVID-19 pandemic had already caused >20 million confirmed infections and >750,000 documented deaths across 216 countries, according to World Health Organization online updates (https://www.who.int/emergencies/diseases/novel-coronavirus-2019). There are currently no vaccines or effective targeted therapeutics available for this disease (14, 15). It is therefore necessary to study the host range of SARS-CoV-2, because some domestic animals may harbor and spread the virus. Receptor binding is a critical determinant for the host range of coronaviruses (6, 16). SARS-CoV-2 utilizes ACE2, the SARS-CoV receptor (17), as an essential cellular receptor to infect cells (8, 18, 19). Studying the ability of SARS-CoV-2 and its related pangolin and bat coronaviruses to utilize animal orthologs of ACE2 might provide insight into identifying potential animal hosts, finding new model animals, and developing broadly effective prophylaxis and therapeutics for these viruses.

In this study, we characterized 16 ACE2 orthologs for their function to support entry of SARS-CoV-2, as well as that of SARS-CoV, Bat-CoV RaTG13 (8), and Pangolin-CoV-2020 (11). To explore broadly anticoronavirus approaches to treatment and prevention of these viruses, we evaluated recombinant IgG Fc-fusion variants of spike-protein receptor-binding domains (RBD-Ig) and soluble ACE2 (ACE2-Ig) for their neutralization potency against pseudotypes of these related but diverse viruses, as well as SARS-CoV-2 live virus.

RESULTS

A wide range of ACE2 orthologs support binding to RBD proteins of four coronaviruses. The RBD of SARS-CoV-2, like that of SARS-CoV, mainly relies on residues in its RBM to bind ACE2 (Fig. 1A) (20–22). Some of these residues are also conserved in the RBDs of Pangolin-CoV-2020 and Bat-CoV RaTG13 (Fig. 1B). Through analyzing ACE2 residues that are within 5 Å from SARS-CoV-2 RBD atoms, we found that these residues are highly conserved across the 16 analyzed ACE2 orthologs, including human ACE2 and ACE2 orthologs of 15 domestic and wild animals (Fig. 1A and C, Table 1), indicating that a substantial proportion of these orthologs might be able to bind RBDs of these diverse but related coronaviruses. We then constructed expression plasmids for the 16 ACE2 orthologs and expressed mouse IgG2 Fc fusion proteins of the RBDs of SARS-

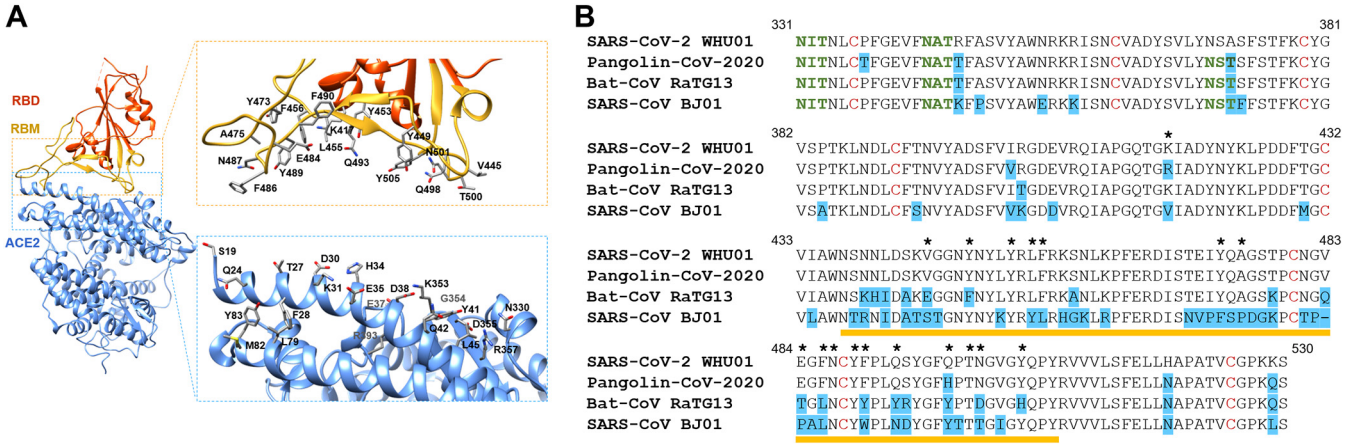

FIG 1 SARS-CoV-2 and ACE2 contact residues are conserved among four SARS-like viruses and 16 ACE2 orthologs, respectively. (A) Interactions between the SARS-CoV-2 receptor binding domain (RBD, red) and ACE2 (blue) involve a large number of contact residues (PDB accession no. 6M0J). RBD residues <5 Å from ACE2 atoms and ACE2 residues <5 Å from RBD atoms are shown. (B) The sequences of the SARS-CoV-2 WHU01, a pangolin coronavirus identified in *Manis javanica* (Pangolin-CoV-2020), a bat coronavirus identified in *R. affinis* (Bat-CoV RaTG13), and the SARS-CoV BJ01 are aligned, with residues different from the corresponding ones in SARS-CoV-2 highlighted in blue. The stars indicate RBD residues <5 Å from ACE2 atoms. The yellow lines indicate the RBM region. N-linked glycosylation motifs are indicated in green. (C) Sequences of ACE2 orthologs from the 16 indicated species are aligned, with only residues <5 Å from RBD atoms shown here. The numbering is based on human ACE2 protein, and the residues different from the corresponding ones in human ACE2 are highlighted in blue.

CoV-2 WHU01, Pangolin-CoV-2020, Bat-CoV RaTG13, and SARS-CoV BJ01. Purified RBD proteins were then used to perform surface staining of 293T cells transfected with each of the 16 ACE2 orthologs or a vector plasmid control (Fig. 2). All of the RBD proteins showed binding to a number of ACE2 orthologs. Unexpectedly, although the SARS-

TABLE 1 Species and accession numbers of ACE2 orthologs investigated in this study

No.	Species name used in the text	Binomial name	NCBI reference sequence ID or GenBank ID
1	Human	*Homo sapiens*	NM_021804.3
2	Camel	*Camelus bactrianus*	XM_010968001.1
3	Cattle	*Bos taurus*	NM_001024502.4
4	Horse	*Equus caballus*	XM_001490191.5
5	Donkey	*Equus asinus*	XM_014857647.1
6	Goat	*Capra hircus*	NM_001290107.1
7	Sheep	*Ovis aries*	XM_012106267.3
8	Cat (domestic)	*Felis catus*	NM_001039456.1
9	Rabbit	*Oryctolagus cuniculus*	XM_002719845.3
10	Guinea pig (domestic)	*Cavia porcellus*	XM_023562040.1
11	Pangolin	*Manis javanica*	XM_017650257.1
12	Civet	*Paguma larvata*	GQ262789.1
13	Bat	*Rhinolophus sinicus* (isolate Rs-3357)	KC881004.1
14	Rat	*Rattus norvegicus*	NM_001012006.1
15	Mouse	*Mus musculus*	NM_027286.4
16	Chicken	*Gallus gallus*	MK560199.1

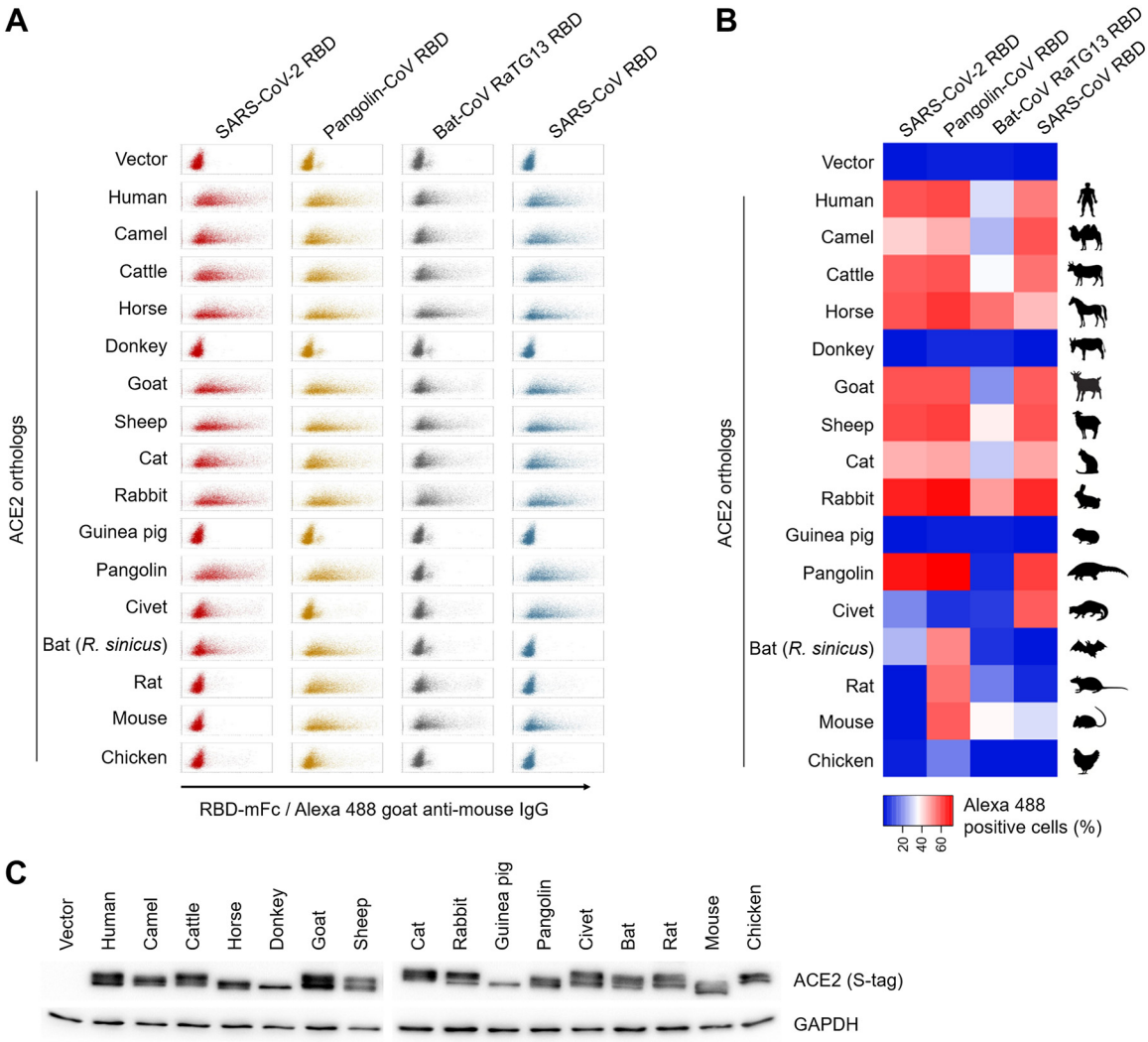

FIG 2 A wide range of ACE2 orthologs support binding to RBD proteins of SARS-CoV-2 and three related coronaviruses. (A) 293T cells were transfected with adjusted amounts of the indicated ACE2-ortholog plasmids to have similar expression levels of the ACE2 ortholog proteins. Cells were then stained with an RBD-mouse IgG2 Fc fusion protein of SARS-CoV-2 WHU01, Pangolin-CoV-2020, Bat-CoV RaTG13, or SARS-CoV BJ01, followed by staining with an Alexa 488-goat anti-mouse IgG secondary antibody. RBD-ACE2 binding was detected using flow cytometry. (B) Percentages of cells positive for RBD binding in panel A are presented as a heatmap according to the indicated color code. (C) Expression levels of the indicated ACE2 orthologs were detected using Western blotting. The data shown are representative of two independent experiments performed by two different people with similar results.

CoV-2 and SARS-CoV RBDs differ significantly in the RBM region and ACE2-contact residues, both RBDs bound to 11 ACE2 orthologs with 10 identical ones. Moreover, the Pangolin-CoV-2020 RBD, which differs from SARS-CoV-2 RBD with only one amino acid within the RBM region, kept nine SARS-CoV-2 RBD-interacting ACE2 orthologs and gained three additional interacting ones, including that of rat, mouse, and chicken. The RBD of Bat-CoV RaTG13 then showed a binding profile significantly different and narrower than the other three RBDs. Note that human ACE2 and ACE2 orthologs of some domestic animals, including camels, cattle, horses, goats, sheep, cats, and rabbits, support efficient binding to all the four tested RBDs, suggesting that these ACE2 orthologs might be generally functional for supporting cell entry of the four tested viruses.

A wide range of ACE2 orthologs can support entry of the four coronaviruses. To evaluate spike protein-mediated entry of these coronaviruses, we generated retrovirus-based luciferase reporter pseudoviral particles (pp) enveloped with one of six different spike proteins, including a wild-type SARS-CoV-2 spike (SARS-CoV-2 WHU01

pp), a furin site deletion mutant of SARS-CoV-2 spike (SARS-CoV-2 Δfurin pp), a wild-type SARS-CoV spike (SARS-CoV BJ01 pp), a SARS-CoV spike carrying the Pangolin-CoV-2020 RBD (Pangolin-RBD/BJ01 pp), a wild-type Bat-CoV spike (Bat-CoV RaTG13 pp), and a Bat-CoV spike carrying the Pangolin-CoV-2020 RBD (Pangolin-RBD/RaTG13 pp). These reporter pseudoviruses were used to infect 293T cells expressing each of the 16 ACE2 orthologs. A vesicular stomatitis virus protein G (VSV-G)-pseudotyped reporter retrovirus whose entry is independent of ACE2 was used as a control virus. As expected, all the orthologs that supported RBD binding were also functional on supporting pseudovirus infection. Again, ACE2 orthologs of humans and most domestic mammals, including camels, cattle, horses, goats, sheep, cats, and rabbits, supported entry of all the tested pseudoviruses (Fig. 3A to G). It is of note that, although furin-cleaved and uncleaved SARS-CoV-2 spike trimers have significant structural difference (23), infection with SARS-CoV-2 Δfurin pseudovirus produced stronger reporter signals but an almost identical pattern of ACE2-ortholog usage as the wild-type pseudovirus (Fig. 3A and B). These data are consistent with the findings that both furin-cleaved and uncleaved SARS-CoV-2 spike trimers can adopt an ACE2-binding-competent conformation albeit at different frequency (17 to 50%), and furin cleavage reduces overall stability of the spike protein (23–25). The ability of ACE2 orthologs to support SARS-CoV-2 infection was further confirmed by infection assays using SARS-CoV-2 live virus (Fig. 3H). These data indicate that humans and these domestic animals might be generally susceptible to infections of the four distinct coronaviruses.

ACE2-Ig variants that have soluble ACE2 domain truncated at residue 740 but not 615 potently block SARS-CoV-2 entry. Recombinant RBD and soluble ACE2 proteins have been shown to potently block SARS-CoV entry (26, 27). To investigate whether similar approaches could also be applied to SARS-CoV-2, we first produced mouse IgG2a Fc fusion proteins of RBD (RBD-Ig) and soluble ACE2 (ACE2-Ig) variants (Fig. 4A). Specifically, the RBD variants include wild-type RBDs of SARS-CoV, Pangolin-CoV-2020, and SARS-CoV-2, and four mutants of SARS-CoV-2 RBD that were expected to bind ACE2 better via additional possible aromatic-stacking (F486W, Y505W) or salt-bridge (K417R, G496D) interactions. The ectodomain of cell-surface ACE2 spanning its residues 18 to 740 contains an enzymatic domain (18-615) and a Collectrin-like domain (CLD). Previous crystal-structure studies showed that soluble ACE2 protein truncated at its residue 615, preceding the CLD domain, express well and forms stable complex with the RBD of SARS-CoV and SARS-CoV-2, respectively (21, 22). Therefore, the ACE2-Ig variants include human ACE2 truncated at its residue 615 (615-wt) and 740 (740-wt), respectively, and mutants of the 615- and 740-version ACE2-Ig proteins that were expected to inactivate ACE2s' enzymatic activity (NN) or bind SARS-CoV-2 RBD better via additional possible hydrophobic (Y83W, H34Y, M82K) or salt-bridge (D30E) interactions. We then evaluated these proteins for their potency of blocking SARS-CoV-2 Δfurin pseudovirus infection (Fig. 4B and C). Among all the RBD-Ig variants, the Y505W mutant of SARS-CoV-2 RBD showed modestly improved potency over the wild type, and wild-type RBD of Pangolin-CoV-2020 showed the best neutralization activity among all the tested RBDs (Fig. 4B). Among the tested ACE2-Ig variants, interestingly, all the 740-version variants showed significantly better potency than the 615-version variants (two-tailed two-sample *t* test, $P < 0.001$; Fig. 4C). In addition, D30E mutants of both 615- and 740-version proteins showed improved potency over the corresponding wild types (two-sample *t* test, $P < 0.01$), and the 740-D30E variant outperformed all the RBD-Ig and ACE2-Ig variants.

The 740-D30E variant of ACE2-Ig is a broadly neutralizing immunoadhesin. We further tested the 740-wt and 740-D30E variants of ACE2-Ig for their neutralization activities against SARS-CoV-2, SARS-CoV, Pangolin-CoV-2020, and Bat-CoV RaTG13 pseudotypes (Fig. 5). Interestingly, the D30E mutation improved the protein's neutralization activity against SARS-CoV-2 and Bat-CoV RaTG13 pseudoviruses (two-sample *t* test, $P < 0.01$; Fig. 5A and C) but not Pangolin-RBD/BJ01 or SARS-CoV pseudovirus (two-sample *t* test, $P > 0.05$; Fig. 5B and D). The D30 residue of human ACE2 was

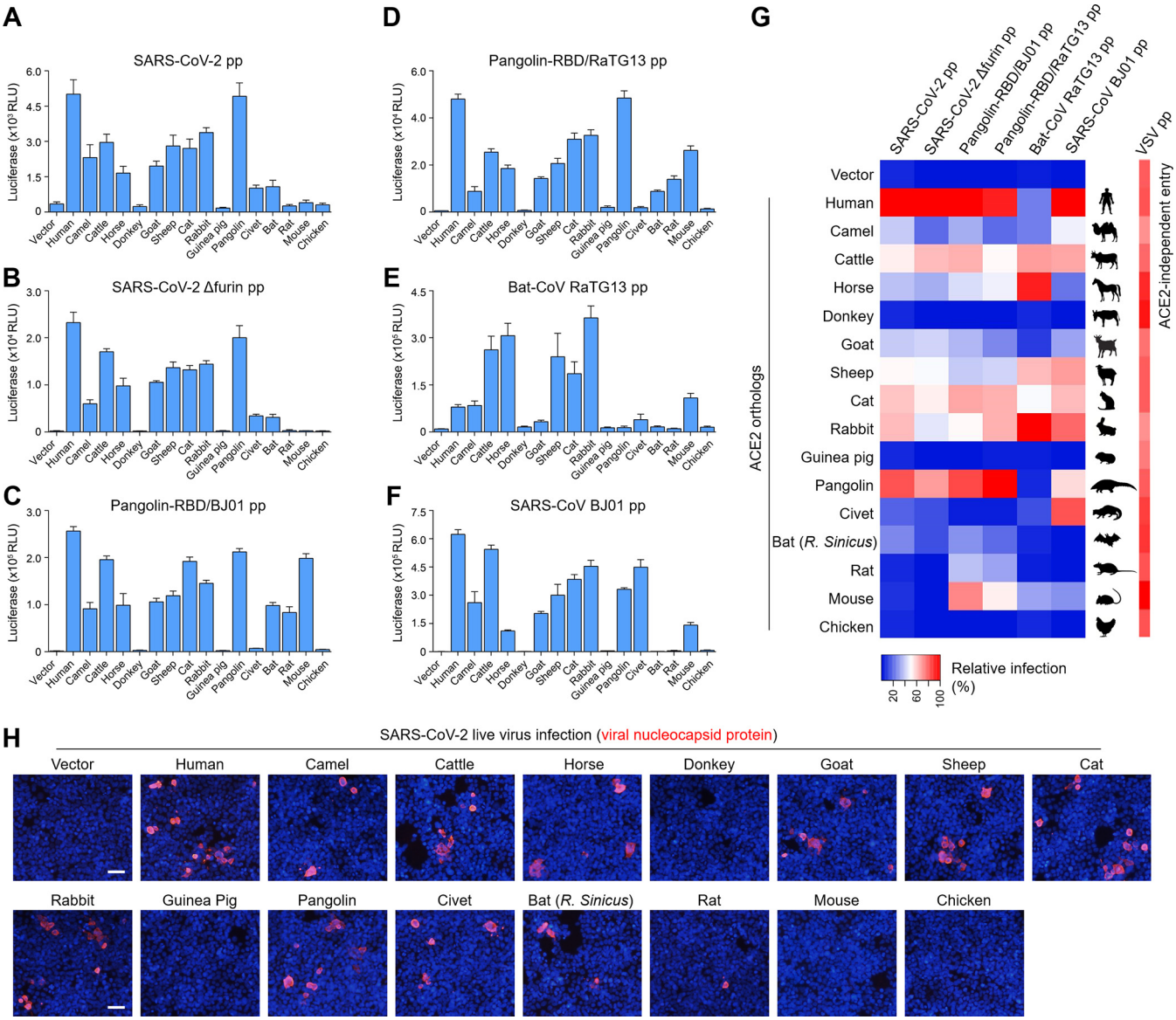

FIG 3 A wide range of ACE2 orthologs support cell entry of SARS-CoV-2 and three related coronaviruses. (A to F) 293T cells in 96-well plates were transfected with adjusted amounts of the indicated ACE2-ortholog plasmids to have similar expression levels of the ACE2 ortholog proteins. Cells were then infected with retrovirus-based luciferase reporter pseudoviral particles (pp) enveloped with the indicated spike proteins. ACE2 ortholog-mediated viral entry was measured by luciferase reporter expression at 48 h (A to D and F) or 60 h (E) postinfection. (G) The relative infection (%) values for each ACE2 ortholog-mediated viral entry shown in panels A to F were independently calculated against the highest expression values of the same pseudotype panel and are presented as a heatmap according to the indicated color code. (H) 293T cells expressing ACE2 orthologs of the indicated species were infected with SARS-CoV-2 live virus at 800 $TCID_{50}$. Cells were then fixed and stained with rabbit anti-SARS-CoV-2 nucleocapsid (NP) polyclonal antibody for fluorescence microscopy at 24 h postinfection. Red indicates SARS-CoV-2 NP, and blue indicates cell nuclei. Scale bars, 50 μm. The data shown are representative of two or three experiments independently performed by two different people with similar results, and data points in panels A to F represent the means ± the SD of four biological replicates.

consistently found to form a salt-bridge interaction with the K417 residue of SARS-CoV-2 RBD in multiple released structures of SARS-CoV-2 RBD in complex with ACE2 (20, 21) (Fig. 5E). The residue 417 of Bat-CoV RaTG13 is also a lysine, while the same residue is an arginine for Pangolin-CoV-2020 RBD and a valine for SARS-CoV RBD. Thus, the mechanism of the D30E-mediated improvement is likely that the mutation enhances the salt-bridge interaction between the residue 30 of the ACE2 and residue 417 of SARS-CoV-2 and Bat-CoV RaTG13 RBDs. These data suggest that the 740-D30E variant of ACE2-Ig is a broadly neutralizing immunoadhesin against SARS-CoV-2, SARS-CoV, Pangolin-CoV-2020, and Bat-CoV RaTG13.

An antibody-like ACE2-Ig variant further improves neutralization potency by ~10-fold. To obtain a more potent ACE2-Ig that may serve as an anti-SARS-CoV-2 drug

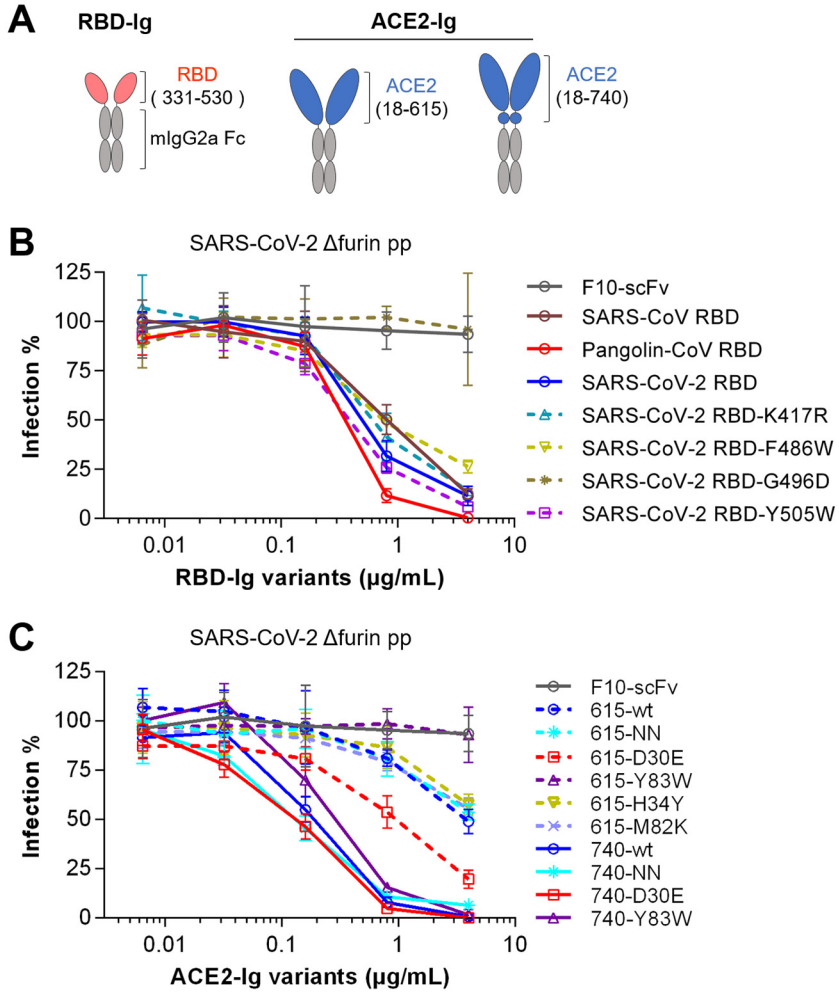

FIG 4 Recombinant RBD-Ig and ACE2-Ig variants efficiently block SARS-CoV-2 entry. (A) Diagrams of RBD-Ig and ACE2-Ig fusion proteins used in the following studies. (B and C) ACE2-expressing 293T cells were infected with SARS-CoV-2 spike-pseudotyped retrovirus (pp) in the presence of purified recombinant RBD-Ig (B) and ACE2-Ig (C) fusion proteins at the indicated concentrations. An Fc fusion protein of an anti-influenza HA antibody, F10-scFv, was used as a control protein here. Viral entry was measured by the luciferase reporter at 48 h postinfection. Luminescence values observed at each concentration were divided by the values observed at concentration zero to calculate the percent infection (Infection%) values. Note that all the 740-version variants showed significantly better potency than the 615-version variants (two-tailed two-sample *t* test, $P < 0.001$). The data shown are representative of two experiments independently performed by two different people with similar results, and data points represent the means ± the SD of four biological replicates.

candidate, we generated more variants and used human IgG1 domains to replace the mouse counterparts in the ACE2-Ig fusion proteins. Two new variants, which have an antibody like configuration and contain four or six soluble ACE2 domains in a single molecule, are named as ACE2-Ig-v3 and ACE2-Ig-v4, respectively (Fig. 6A). We first tested these variants for their neutralization potency against SARS-CoV-2 pseudovirus. Both of the new variants showed pronounced improvements over ACE2-Ig-v1.1, the original 740-D30E dimer variant (Fig. 6A to C). Specifically, ACE2-Ig-v3 and ACE2-Ig-v4 have estimated 50% inhibitory concentration (IC_{50}) values of 40 to 70 pM and IC_{90} values of 250 to 730 pM, representing >10-fold improvement on IC_{50} and >25-fold improvement on IC_{90} compared to those of ACE2-Ig-v1.1 (Fig. 6B and C). Because the ACE2-Ig-v4 configuration significantly impairs protein yield during production (data not shown), we chose to proceed with ACE2-Ig-v3 to test its neutralization potency against SARS-CoV-2 live virus (Fig. 6D). Consistent with the pseudovirus neutralization data, ACE2-Ig-v3 at 0.16 μg/ml showed a more potent inhibition of SARS-CoV-2 live virus

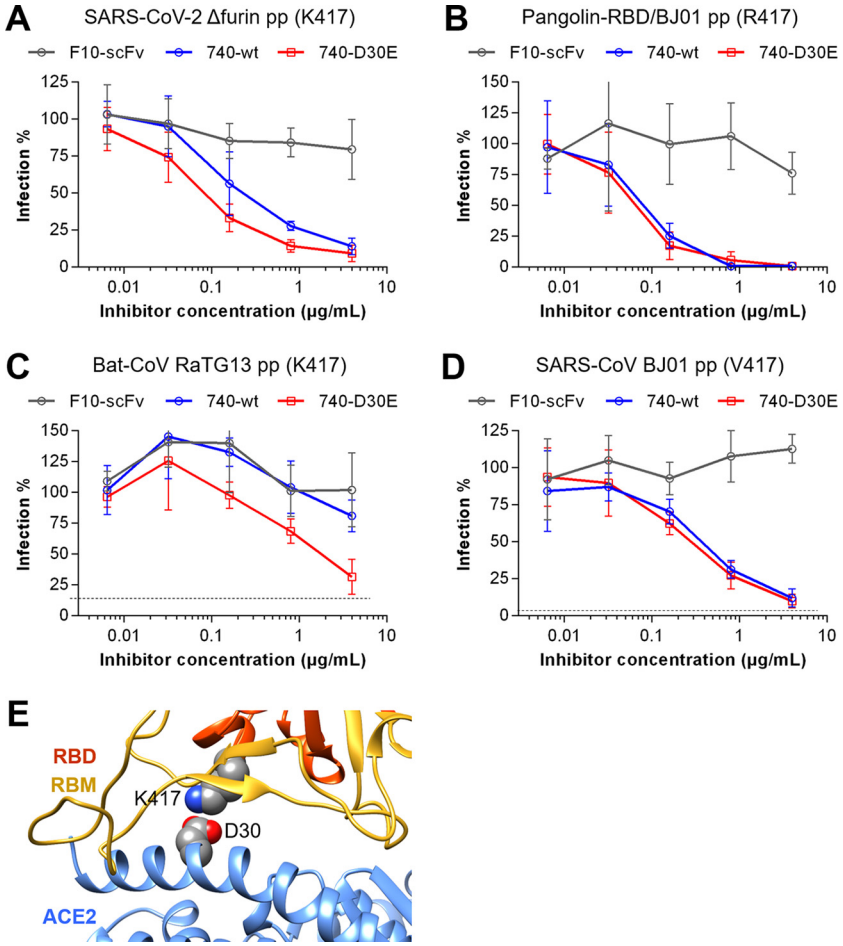

FIG 5 The 740-D30E variant of ACE2-Ig broadly neutralizes entry of SARS-CoV-2, SARS-CoV, Pangolin-CoV-2020 and Bat-CoV RaTG13. (A to D) Human ACE2-expressing 293T were infected with the indicated pseudotypes in the presence of an Fc fusion protein, F10-scFv (gray), ACE2 740-wt (blue), or ACE2 740-D30E (red). Viral entry was measured by luciferase reporter expression at 48 h (A, B, and D) or 60 h (C) postinfection, and the percent infection (Infection%) values were calculated. Note that the D30E mutation on the ACE2-Ig protein improved the protein's neutralization activity against SARS-CoV-2 (A) and RaTG13 (C) but not Pangolin-CoV-2020 (B) or SARS-CoV (D). The dashed line in panels C and D indicates the background luciferase signals detected in the pseudovirus-infected parental 293T cells. (E) Human ACE2 residue D30 forms a salt bridge with the SARS-CoV-2 RBD residue K417 (PDB accession no. 6M0J). SARS-CoV-2 and RaTG13 have a K417 residue at their spike proteins, while Pangolin-CoV has an R417 residue and SARS-CoV has a V417 residue at their spike proteins, respectively. Thus, a stabilized salt bridge interaction between E30 of the ACE2-Ig protein and K417 of the virus spike protein is likely responsible for the D30E mutation-mediated neutralization enhancement. The data shown are representative of two or three experiments independently performed by two different people with similar results, and data points in panels A to D represent the means ± the SD of three or four biological replicates.

infection than ACE2-Ig-v1 at 0.8 μg/ml. Moreover, ACE2-Ig-v3 at 0.8 μg/ml (1.85 nM) already completely abolished viral nucleocapsid protein (NP) immunofluorescent signal. These data demonstrate that ACE2-Ig-v3 is a markedly improved ACE2-Ig variant as a potent entry inhibitor against SARS-CoV-2 virus.

DISCUSSION

In this study, we investigated the ability of SARS-CoV-2 to utilize animal orthologs of ACE2 for cell entry. We observed that ACE2 orthologs of a wide range of domestic animals, including camels, cattle, horses, goats, sheep, cats, and rabbits, efficiently supported binding and entry of this virus, suggesting that these domestic mammals might be susceptible to this viral infection (Fig. 2B and Fig. 3G). Consistent with this, during preparation of the manuscript, two studies independently reported laboratory

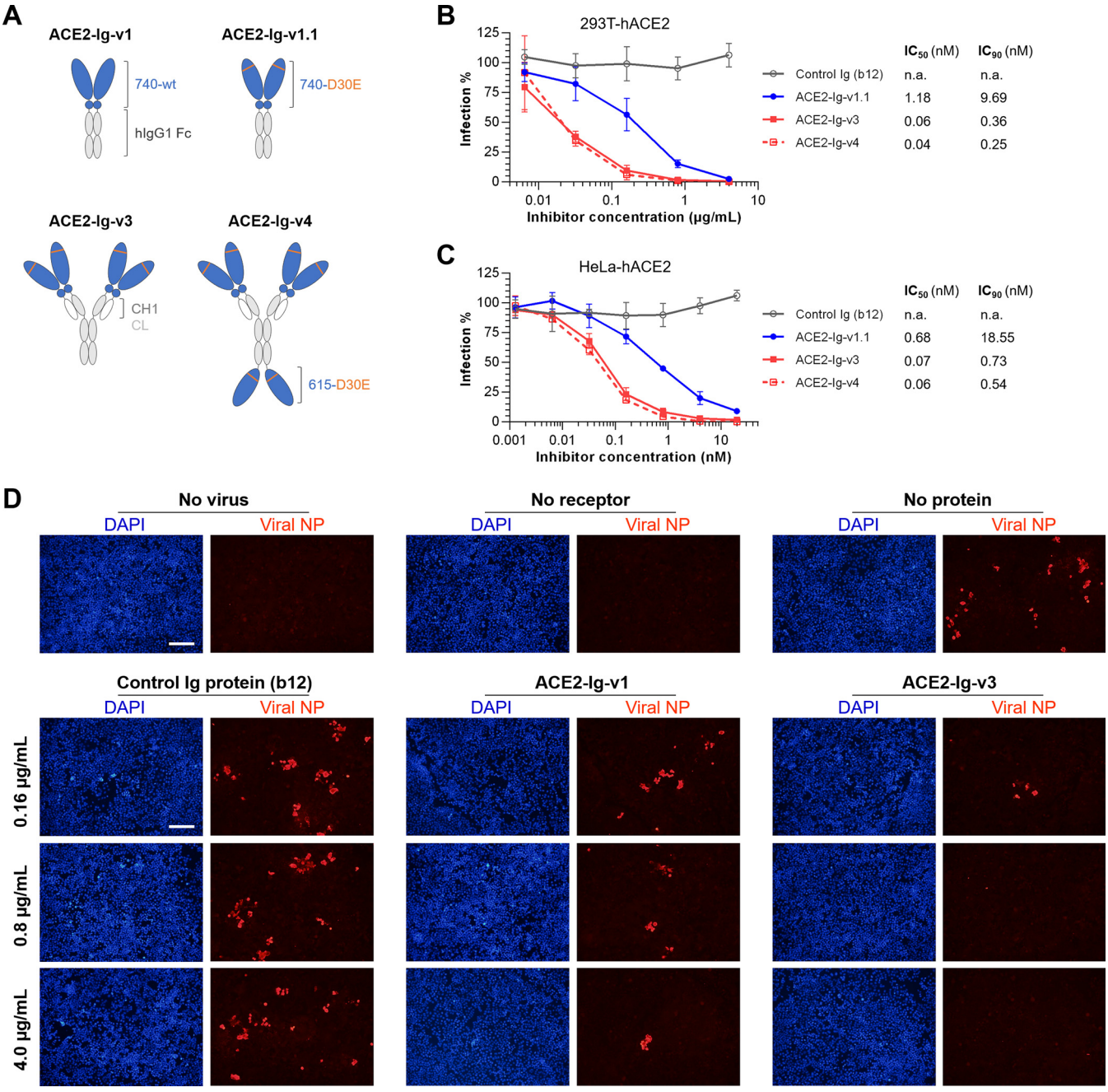

FIG 6 A further improved ACE2-Ig variant with an antibody-like configuration potently neutralizes SARS-CoV-2 live virus. (A) Diagrams of ACE2-Ig variants characterized in the following studies. CH1, IgG heavy-chain constant region 1; CL, human antibody kappa light-chain constant region. (B and C) Human ACE2-expressing 293T (B) or HeLa (C) cells were infected with SARS-CoV-2 pseudotype in the presence of the indicated human IgG1 Fc fusion proteins at the indicated concentrations. An anti-HIV antibody b12 was used as a human IgG1 control. Viral entry was measured by luciferase reporter expression at 48 h postinfection, and the percent infection (Infection%) values were calculated. Estimated IC_{50} and IC_{90} values for each protein are directly derived from the curves and are shown to the right of the figures. (D) Human ACE2-expressing HeLa cells were infected with SARS-CoV-2 live virus at 800 $TCID_{50}$ in the presence of the b12 control protein, ACE2-Ig-v1, or ACE2-Ig-v3 at the indicated concentrations. Cells were then fixed and stained with rabbit anti-SARS-CoV-2 NP polyclonal antibody for fluorescence microscopy at 24 h postinfection. Red indicates SARS-CoV-2 NP and blue indicates cell nuclei. Scale bars, 200 μm. Note that ACE2-Ig-v3 at 0.8 μg/ml (1.85 nM) completely abolished viral NP signal. The data shown are representative of two or three experiments independently performed by two different people with similar results, and data points in panels B and C represent the means ± the SD of three biological replicates.

and natural infection of cats by SARS-CoV-2 (28, 29). Therefore, it is necessary to further investigate the susceptibility of these domestic animals to SARS-CoV-2. In addition to the species investigated in this study, farmed mink has been found susceptible to SARS-CoV-2 and able to transmit the virus back to humans (30, 31). The currently

available information therefore suggests that surveillance of livestock and farmed mammals in marketplaces for SARS-CoV-2 infection might be necessary.

Pangolins have been proposed as potential intermediate or natural hosts of SARS-CoV-2 (11–13). It has been proposed that SARS-CoV-2 might originate from recombination of a Pangolin-CoV-like coronavirus and a RaTG13-like coronavirus (13, 32). Thus, the intermediate host of SARS-CoV-2 should also be susceptible to both of the "parental viruses." Here, we found that pangolin (*Manis javanica*) ACE2 does not support binding or entry of Bat-CoV RaTG13, a coronavirus known to have the highest genome sequence identity (96.2%) to SARS-CoV-2 so far, suggesting a lower likelihood of Malayan pangolins (*Manis javanica*) being intermediate hosts for SARS-CoV-2. On the other hand, we also found that SARS-CoV-2, SARS-CoV, and Pangolin-CoV-2020 (11) can all efficiently utilize pangolin (*Manis javanica*) ACE2 for cellular binding and entry, supporting the hypothesis that pangolins might be natural hosts of SARS-CoV-like coronaviruses (11, 12). It is also noteworthy that Pangolin-CoV-2020 can also efficiently utilize human ACE2, as well as a wide range of domestic- and wild-animal ACE2 orthologs for cell entry (Fig. 2B and 3G), indicating that this virus has very broad host range and high risk of spillover into human population in the future.

Animal models are essential for preclinical evaluation of efficacy and potential toxicity of candidate prophylactic vaccines or therapeutics for COVID-19, as well as for studying the transmission, pathogenesis, and immunology of this disease. In this study, rabbit ACE2 was found to efficiently support binding and entry of all the four coronaviruses (Fig. 2B and 3G). It is therefore worth exploring whether rabbit, a commonly used laboratory species, could serve as a common model animal for studying COVID-19, SARS, and diseases caused by other SARS-related coronaviruses. Adaptation of viruses to infect mice is another way of developing small animal models of COVID-19. We found in this study that Pangolin-CoV-2020, whose RBM only differs from that of SARS-CoV-2 with one amino acid, could efficiently utilize mouse ACE2 for binding and cell entry (Fig. 1B, 2B, and 3G). These data suggest that mice might be susceptible to this viral infection, and thus this pangolin coronavirus could be used as a surrogate to SARS-CoV-2 for *in vivo* studies in wild-type mice.

Effective vaccines or targeted therapeutics against SARS-CoV-2 infections are not yet available (15). ACE2-Ig that has soluble ACE2 truncated at its residue 615 had been proposed as a candidate therapeutic for SARS-CoV-2 infection in the beginning of the COVID-19 pandemic (33). Two recently posted experimental studies by Lui et al. (34) and Case et al. (35) have also investigated the use of this 615-version ACE2-Ig to block SARS-CoV-2 infection and showed IC_{50} values of $\sim$1 and 29 μg/ml, respectively. Consistent with these studies, we got in our study an estimated IC_{50} value of $\sim$4 μg/ml for this variant (615-wt in Fig. 4C). It is noteworthy that our studies here have identified three key improvements over the 615-version ACE2-Ig. First, the 740-wt ACE2-Ig variant showed a $>$20-fold potency improvement over the 615-wt variant, and all the 740-version variants showed markedly enhanced neutralization potency over the 615-version variants (Fig. 4C). The reason for this improvement is not very clear yet, but it is possible that the CLD domain, included in the 740 version, stabilizes an orientation of the ACE2 enzymatic domain favorable to S-protein binding, or that the CLD has an independent anti-SARS-CoV-2 activity. Second, likely because SARS-CoV-2 has adapted in animals (e.g., pangolins) whose ACE2 orthologs have a glutamic acid at position 30, the D30E mutation further improves the 740-version ACE2-Ig's neutralization potency against SARS-CoV-2. Moreover, the D30E mutation also enables the protein to neutralize all the four distinct SARS-like coronaviruses (Fig. 5). Third, by utilizing an antibody-like structure to build an ACE2 tetramer, we generated a variant ACE2-Ig-v3 that has at least 10-fold additional improvement on neutralization potency against SARS-CoV-2 pseudotype as well as live virus (Fig. 6). Through these changes, we have therefore successfully improved the originally very modest immunoadhesin inhibitor ($IC_{50} \approx$ 18 nM) to be a very potent entry inhibitor ($IC_{50} \approx$ 60 pM) against SARS-CoV-2.

Recently, a clinical-grade recombinant soluble ACE2 protein has been shown to block SARS-CoV-2 infection in engineered human organoid (36). A phase 2 clinical trial

to investigate this protein, injected twice daily, as a treatment for COVID-19 patients has already started recruiting patients in multiple countries (https://clinicaltrials.gov/ct2/show/NCT04335136). Considering that fusion with IgG Fc improves soluble ACE2 protein's half-life in mice from <2 h to over a week (37, 38) and that we have markedly improved the neutralization potency of ACE2-Ig, we therefore optimistically expect that the improved ACE2-Ig variants described in this study could potentially be developed to provide effective protections from SARS-CoV-2 and other SARS-like viruses that might spillover into humans in the future, as well as SARS-CoV-2 variants that emerge over the course of the current pandemic.

MATERIALS AND METHODS

Ethics statement. All experiments involving SARS-CoV-2 live virus infections were approved (no. QS2020050050) by the ethics committee of Shenzhen Center for Disease Control and Prevention (SZCDC) and the ethics committee of Shenzhen Bay Laboratory. SARS-CoV-2 live virus was isolated from SARS-CoV-2 RNA RT-qPCR-positive oropharyngeal swab samples by SZCDC, and all SARS-CoV-2 live virus experiments were performed in the biosafety level 3 facility at SZCDC.

Cells. 293T cells and Vero cells were kindly provided by Stem Cell Bank, Chinese Academy of Sciences, confirmed mycoplasma-free by the provider, and maintained in Dulbecco modified Eagle medium (DMEM; Life Technologies) at 37°C in a 5% CO_2-humidified incubator. Growth medium was supplemented with 2 mM GlutaMAX-I (Gibco, catalog no. 35050061), 100 μM nonessential amino acids (Gibco, catalog no. 11140050), 100 U/ml penicillin and 100 μg/ml streptomycin (Gibco, catalog no. 15140122), and 10% FBS (Gibco, catalog no. 10099141C). 293T-based stable cells expressing human ACE2 were maintained under the same culture condition as 293T, except that 3 μg/ml of puromycin was added to the growth medium. 293F cells for recombinant protein production were generously provided by Yu J. Cao (School of Chemical Biology and Biotechnology, Peking University Shenzhen Graduate School) and maintained in SMM 293-TII serum-free medium (Sino Biological, catalog no. M293TII) at 37°C, 8% CO_2, in a shaker incubator at 125 rpm.

Plasmids. DNA fragments encoding spike proteins of SARS-CoV-2 WHU01 (GenBank accession no. MN988668.1), SARS-CoV BJ01 (GenBank AY278488.2), Pangolin-CoV (National Genomics Data Center GWHABKW00000000; https://bigd.big.ac.cn/search/?dbId=gwh&q=GWHABKW00000000&page=1) (11), and Bat-CoV RaTG13 (GenBank MN996532) (8), were synthesized by the Beijing Genomic Institute (BGI, China) and Sangon Biotech (Shanghai, China) and then cloned into pcDNA3.1(+) plasmid or pCAGGS plasmid between EcoRI and XhoI restriction sites. Plasmids encoding recombinant RBD and soluble ACE2 variants were generated by cloning each of the gene fragments into a pCAGGS-based mouse-IgG2a or human IgG1 Fc fusion protein expression plasmid between NotI and BspEI sites. The retroviral reporter plasmids encoding a Gaussia luciferase or a green fluorescent protein (GFP) reporter gene were constructed by cloning the reporter genes into pQCXIP plasmid (Clontech), respectively. DNA fragments encoding C-terminally S-tagged ACE2 orthologs were synthesized in pUC57 backbone plasmid by Sangon Biotech (Shanghai, China). These fragments were then cloned into pQCXIP plasmid (Clontech) between SbfI and NotI restriction sites.

IgG Fc fusion protein production and purification. 293F cells at the density of 6×10^5 cells/ml were seeded into 100 ml of SMM 293-TII serum-free medium (Sino Biological, catalog no. M293TII) 1 day before transfection. The cells were then transfected with 100 μg of plasmid in complex with 250 μg of PEI MAX 4000 (Polysciences, Inc., catalog no. 24765-1). Cell culture supernatants were collected at 48 to 72 h posttransfection. Recombinant Fc fusion proteins are purified using protein A-Sepharose CL-4B (GE Healthcare, catalog no. 17-0780-01), eluted with 0.1 M citric acid at pH 4.5, and neutralized with 1 M Tris-HCl at pH 9.0. Buffers were then exchanged to phosphate-buffered saline (PBS), and proteins were concentrated by 30-kDa cutoff Amicon Ultra-15 centrifugal filter units (Millipore, catalog no. UFC903096).

Flow cytometry for detecting interactions of RBD-Ig proteins with cell surface ACE2 orthologs. 293T cells were seeded at 20% density in 48-well plates at 12 to 15 h before transfection. Cells in each well were then transfected with 0.5 μl of Lipofectamine 2000 (Life Technologies, catalog no. 11668019) in complex with 200 ng of plasmid encoding one of the 16 ACE2 orthologs or a D30E mutant of the human ACE2. Culture medium was changed at 6 h after transfection. Cells were then detached with 5 mM EDTA (Life Technologies, catalog no. 15575020) at 36 h posttransfection. The cells were then stained with 5 μg/ml RBD-Ig proteins at 37°C for 10 min, washed three times, and then stained with 2 μg/ml Alexa488-conjugated goat anti-mouse IgG secondary antibody (Invitrogen, catalog no. A-11001) at room temperature for 20 min. After another three washes, cells were analyzed by Attune NxT flow cytometer (Thermo Fisher), and signals of 10,000 FSC/SSC-gated cells were collected for each sample.

Western Blot to detect S-tagged ACE2 (ACE2-S-tag) or C9-tagged spike (Spike-C9-tag) expression in 293T cells. 293T cells were seeded at 20% density in 6-well plates at 12 to 15 h before transfection. Cells in each well were then transfected with 2 μg of plasmid in complex with 5 μl of Lipofectamine 2000 (Life Technologies, catalog no. 11668019). At 36 h after transfection, the cells were lysed, and 10 μg of total protein was used for Western blotting. ACE2-S-tag expression was detected by using 6.2, a mouse anti-S-tag monoclonal antibody (Invitrogen, catalog no. MA1-981), and a horseradish peroxidase (HRP)-conjugated goat anti-mouse IgG Fc secondary antibody (Invitrogen, catalog no. 31437). Beta-actin was used as an internal control. Spike-C9-tag expression was then detected by using 1D4, a mouse anti-C9-tag monoclonal antibody (Invitrogen, catalog no. MA1-722), and the HRP-conjugated goat anti-mouse IgG Fc secondary antibody (Invitrogen, catalog no. 31437).

Production of reporter retroviruses pseudotyped with coronavirus spike proteins or VSV-G. MLV retroviral vector-based coronavirus-spike and VSV-G pseudotypes were produced using a previously described protocol (23) with some modifications. 293T cells were seeded at 30% density in 150 mm dish at 12 to 15 h before transfection. Cells were then transfected with 67.5 μg of PEI MAX 4000 (Polysciences, Inc., catalog no. 24765-1) in complex with 11.25 μg of plasmid encoding a coronavirus spike protein or VSV-G, 11.25 μg of plasmid encoding murine leukemia virus) Gag and Pol proteins, and 11.25 μg of a pQCXIP-based GFP or luciferase reporter plasmid. Eight hours after transfection, cell culture medium was refreshed and changed to growth medium containing 2% fetal bovine serum (FBS; Gibco, catalog no. 10099141C) and 25 mM HEPES (Gibco, catalog no. 15630080). Cell culture supernatants were collected at 36 to 48 h posttransfection, spun down at 3,000 $\times$ *g* for 10 min, and filtered through 0.45-μm filter units to remove cell debris. Coronavirus spike-pseudotyped viruses were then concentrated 10 times at 2,000 $\times$ *g* using 100-kDa cutoff Amicon Ultra-15 centrifugal filter units (Millipore, catalog no. UFC910024).

Pseudovirus infection of 293T cells expressing ACE2 orthologs. 293T cells were seeded at 20% density in polylysine precoated 48-well plates 12 to 15 h before transfection. Cells in each well were then transfected with 0.5 μl of Lipofectamine 2000 (Life Technologies, catalog no. 11668019) in complex with 200 ng of a vector control plasmid or a plasmid encoding one of the 16 ACE2 orthologs. Cell culture medium was refreshed at 6 h posttransfection. After another 18 h, the cells in each well were infected with 50 μl of SARS-CoV-2 wild-type pseudovirus (10$\times$ concentrated), 20 μl of SARS-CoV-2 ΔFurin pseudovirus (10$\times$ concentrated), 50 μl of Bat-CoV RaTG13 pseudovirus (10$\times$ concentrated), 10 μl of SARS-CoV pseudovirus (10$\times$ concentrated), or 10 μl of VSV-G pseudovirus diluted in 200 μl of culture medium containing 2% FBS (Gibco, catalog no. 10099141C). The culture medium was refreshed at 2 h after pseudovirus infection, and the medium was refreshed every 12 h. For the luciferase reporter virus-infected cells, the cell culture supernatants were collected and subjected to a Gaussia luciferase assay at 48 h postinfection. The GFP reporter virus-infected cells were stained with Hoechst 33342 (Invitrogen, catalog no. H3570) and subjected to fluorescence microscopy (IX73 microscope; Olympus) at 48 h postinfection.

Gaussia luciferase luminescence flash assay. To measure Gaussia luciferase expression, 20 μl of cell culture supernatant of each sample and 100 μl of assay buffer containing 4 μM coelenterazine native (Biosynth Carbosynth, catalog no. C-7001) were added to one well of a 96-well black opaque assay plate (Corning, catalog no. 3915) and measured with the Tristar5 multifunctional microplate reader (Berthold Technologies) for 0.1 s/well.

Coronavirus pseudovirus neutralization assay. Coronavirus spike protein-pseudotyped luciferase reporter viruses were prediluted in DMEM (2% FBS, heat inactivated) containing titrated amounts of RBD-Ig or ACE2-Ig variant proteins. An Fc fusion protein of an anti-influenza hemagglutinin (HA) antibody, F10-scFv (25), was used as a control protein here. Virus-inhibitor mixtures were then added to ACE2-expressing 293T or HeLa cells in polylysine (Sigma, catalog no. P4832-50ml) precoated 96-well plates and incubated overnight at 37°C. The cells were then washed with serum-free medium and incubated in 150 μl of DMEM (2% FBS) at 37°C. Cell culture supernatants were collected for Gaussia luciferase assay at 48 h postinfection.

SARS-CoV-2 live virus infection of ACE2 ortholog-expressing 293T cells. 293T cells expressing one of the 16 ACE2 orthologs were inoculated with SARS-CoV-2 live virus at 800 50% tissue culture infective dose(s) ($TCID_{50}$) and incubated for 1 h at 37°C. The cells were then washed with serum-free medium and incubated in 150 μl of DMEM (2% FBS) at 37°C for an additional 24 h. The cells were then fixed with 4% paraformaldehyde in PBS, permeabilized with 0.5% Triton X-100, and sequentially stained with 1:200-diluted rabbit anti-SARS-CoV-2 nucleocapsid polyclonal antibody (Sino Biological, catalog no. 40588-T62) at 37°C for 30 min, 4 μg/ml of Alexa Fluor 568 goat anti-rabbit IgG (Invitrogen, catalog no. A-11011) at 37°C for 20 min, and 0.5 μg/ml of DAPI (4′,6′-diamidino-2-phenylindole; Sigma-Aldrich, catalog no. D9542-5mg) at room temperature for 10 min. Stained cells were then examined under fluorescence microscope (IX73 microscope; Olympus).

SARS-CoV-2 live virus neutralization by ACE2-Ig variants. SARS-CoV-2 live virus at 800 $TCID_{50}$ were prediluted in DMEM (2% FBS, heat inactivated) containing titrated amounts of ACE2-Ig variant proteins and incubated at 37°C for 1 h. Virus-inhibitor mixtures were then added to ACE2-expressing 293T or HeLa cells in polylysine-precoated 48-well plates and incubated for 1 h at 37°C. The cells were then washed with serum-free medium and incubated in 400 μl of DMEM (2% FBS) at 37°C for 24 to 40 h. Cells were then fixed for immunofluorescence staining of viral nucleocapsid proteins as described above.

Data collection and analysis. All the experiments were repeated two to four times. All of the infection assays for Fig. 3 were independently performed by two different people, and all the data are reproducible in different hands. The key neutralization assays of Fig. 4 to 6 were independently performed by two or three different people, and all of the data are reproducible in different hands. Attune NxT Software (Thermo Fisher) was used to collect and analyze flow cytometry data. Image Lab Software (Bio-Rad) was used to collect SDS-PAGE and Western blot image data. Cell Sens Software (Olympus) was used to collect fluorescence microscopy data. ICE Software (Berthold Technologies) was used to collect luciferase assay data. GraphPad Prism 6.0 software was used for figure preparation and statistical analyses.

Statistical analysis. Data expressed as mean values $\pm$ the standard deviations (SD). Statistical analyses were performed using two-sided two-sample Student *t* test using GraphPad Prism 6.0 software when applicable. Differences were considered significant at $P < 0.01$.

Data availability. The study did not generate unique data sets or code. Our research resources, including methods, plasmids, and protocols, are available upon reasonable request to qualified academic

investigators for noncommercial research purposes. All reagents developed, such as vector plasmids, as well as detailed methods, will be made available upon written request.

ACKNOWLEDGMENTS

We thank Yu J. Cao (School of Chemical Biology and Biotechnology, Peking University Shenzhen Graduate School, Shenzhen China), for generously providing the 293F cells used for recombinant protein production in this study.

This study was supported by the National Natural Science Foundation of China (8187631, S.F.), the Shenzhen Science and Technology Program, Shenzhen Science and Technology Innovation Commission (JCYJ20180307102005105, S.F.), the Guangdong Provincial Department of Science and Technology, Shenzhen Bay Laboratory COVID-19 Contingency Funds (2020B1111340063, G.Z.; 2020B1111340077, X.Z.; and 2020B1111340078, S.F.), the Key Project of Shenzhen Science and Technology Innovation Commission (202002073000003, R.Z.), and Shenzhen Bay Laboratory Startup Funds (21230041, G.Z.).

We declare that we have no conflicts of interest.

REFERENCES

1. Zeng FY, Chan CW, Chan MN, Chen JD, Chow KY, Hon CC, Hui KH, Li J, Li VY, Wang CY, Wang PY, Guan Y, Zheng B, Poon LL, Chan KH, Yuen KY, Peiris JS, Leung FC. 2003. The complete genome sequence of severe acute respiratory syndrome coronavirus strain HKU-39849 (HK-39). Exp Biol Med (Maywood) 228:866–873. https://doi.org/10.1177/15353702-0322807-13.
2. Chim SS, Tsui SK, Chan KC, Au TC, Hung EC, Tong YK, Chiu RW, Ng EK, Chan PK, Chu CM, Sung JJ, Tam JS, Fung KP, Waye MM, Lee CY, Yuen KY, Lo YM, Group CMSR. 2003. Genomic characterization of the severe acute respiratory syndrome coronavirus of Amoy Gardens outbreak in Hong Kong. Lancet 362:1807–1808. https://doi.org/10.1016/S0140-6736(03)14901-X.
3. Zhong NS, Zheng BJ, Li YM, Poon LLM, Xie ZH, Chan KH, Li PH, Tan SY, Chang Q, Xie JP, Liu XQ, Xu J, Li DX, Yuen KY, Peiris, Guan Y. 2003. Epidemiology and cause of severe acute respiratory syndrome (SARS) in Guangdong, People's Republic of China, in February, 2003. Lancet 362:1353–1358. https://doi.org/10.1016/S0140-6736(03)14630-2.
4. Zhou P, Fan H, Lan T, Yang XL, Shi WF, Zhang W, Zhu Y, Zhang YW, Xie QM, Mani S, Zheng XS, Li B, Li JM, Guo H, Pei GQ, An XP, Chen JW, Zhou L, Mai KJ, Wu ZX, Li D, Anderson DE, Zhang LB, Li SY, Mi ZQ, He TT, Cong F, Guo PJ, Huang R, Luo Y, Liu XL, Chen J, Huang Y, Sun Q, Zhang XL, Wang YY, Xing SZ, Chen YS, Sun Y, Li J, Daszak P, Wang LF, Shi ZL, Tong YG, Ma JY. 2018. Fatal swine acute diarrhoea syndrome caused by an HKU2-related coronavirus of bat origin. Nature 556:255–258. https://doi.org/10.1038/s41586-018-0010-9.
5. Guan Y, Zheng BJ, He YQ, Liu XL, Zhuang ZX, Cheung CL, Luo SW, Li PH, Zhang LJ, Guan YJ, Butt KM, Wong KL, Chan KW, Lim W, Shortridge KF, Yuen KY, Peiris JS, Poon LL. 2003. Isolation and characterization of viruses related to the SARS coronavirus from animals in southern China. Science 302:276–278. https://doi.org/10.1126/science.1087139.
6. Cui J, Li F, Shi ZL. 2019. Origin and evolution of pathogenic coronaviruses. Nat Rev Microbiol 17:181–192. https://doi.org/10.1038/s41579-018-0118-9.
7. Yang YL, Qin P, Wang B, Liu Y, Xu GH, Peng L, Zhou J, Zhu SJ, Huang YW. 2019. Broad cross-species infection of cultured cells by bat HKU2-related swine acute diarrhea syndrome coronavirus and identification of its replication in murine dendritic cells *in vivo* highlight its potential for diverse interspecies transmission. J Virol 93:e01448-01419. https://doi.org/10.1128/JVI.01448-19.
8. Zhou P, Yang XL, Wang XG, Hu B, Zhang L, Zhang W, Si HR, Zhu Y, Li B, Huang CL, Chen HD, Chen J, Luo Y, Guo H, Jiang RD, Liu MQ, Chen Y, Shen XR, Wang X, Zheng XS, Zhao K, Chen QJ, Deng F, Liu LL, Yan B, Zhan FX, Wang YY, Xiao GF, Shi ZL. 2020. A pneumonia outbreak associated with a new coronavirus of probable bat origin. Nature 579:270–273. https://doi.org/10.1038/s41586-020-2012-7.
9. Zhu N, Zhang D, Wang W, Li X, Yang B, Song J, Zhao X, Huang B, Shi W, Lu R, Niu P, Zhan F, Ma X, Wang D, Xu W, Wu G, Gao GF, Tan W, China Novel Coronavirus Investigator Research Team. 2020. A novel coronavirus from patients with pneumonia in China, 2019. N Engl J Med 382:727–733. https://doi.org/10.1056/NEJMoa2001017.
10. Lu R, Zhao X, Li J, Niu P, Yang B, Wu H, Wang W, Song H, Huang B, Zhu N, Bi Y, Ma X, Zhan F, Wang L, Hu T, Zhou H, Hu Z, Zhou W, Zhao L, Chen J, Meng Y, Wang J, Lin Y, Yuan J, Xie Z, Ma J, Liu WJ, Wang D, Xu W, Holmes EC, Gao GF, Wu G, Chen W, Shi W, Tan W. 2020. Genomic characterization and epidemiology of 2019 novel coronavirus: implications for virus origins and receptor binding. Lancet 395:565–574. https://doi.org/10.1016/S0140-6736(20)30251-8.
11. Liu P, Jiang JZ, Wan XF, Hua Y, Li L, Zhou J, Wang X, Hou F, Chen J, Zou J, Chen J. 2020. Are pangolins the intermediate host of the 2019 novel coronavirus (SARS-CoV-2)? PLoS Pathog 16:e1008421. https://doi.org/10.1371/journal.ppat.1008421.
12. Lam TT-Y, Jia N, Zhang Y-W, Shum MH-H, Jiang J-F, Zhu H-C, Tong Y-G, Shi Y-X, Ni X-B, Liao Y-S, Li W-J, Jiang B-G, Wei W, Yuan T-T, Zheng K, Cui X-M, Li J, Pei G-Q, Qiang X, Cheung WY-M, Li L-F, Sun F-F, Qin S, Huang J-C, Leung GM, Holmes EC, Hu Y-L, Guan Y, Cao W-C. 2020. Identifying SARS-CoV-2 related coronaviruses in Malayan pangolins. Nature 583:282–285. https://doi.org/10.1038/s41586-020-2169-0.
13. Xiao K, Zhai J, Feng Y, Zhou N, Zhang X, Zou JJ, Li N, Guo Y, Li X, Shen X, Zhang Z, Shu F, Huang W, Li Y, Zhang Z, Chen RA, Wu YJ, Peng SM, Huang M, Xie WJ, Cai QH, Hou FH, Chen W, Xiao L, Shen Y. 2020. Isolation of SARS-CoV-2-related coronavirus from Malayan pangolins. Nature 583:286–289. https://doi.org/10.1038/s41586-020-2313-x.
14. Li G, De Clercq E. 2020. Therapeutic options for the 2019 novel coronavirus (2019-nCoV). Nat Rev Drug Discov 19:149–150. https://doi.org/10.1038/d41573-020-00016-0.
15. Tang D, Comish P, Kang R. 2020. The hallmarks of COVID-19 disease. PLoS Pathog 16:e1008536. https://doi.org/10.1371/journal.ppat.1008536.
16. Li F. 2013. Receptor recognition and cross-species infections of SARS coronavirus. Antiviral Res 100:246–254. https://doi.org/10.1016/j.antiviral.2013.08.014.
17. Li W, Moore MJ, Vasilieva N, Sui J, Wong SK, Berne MA, Somasundaran M, Sullivan JL, Luzuriaga K, Greenough TC, Choe H, Farzan M. 2003. Angiotensin-converting enzyme 2 is a functional receptor for the SARS coronavirus. Nature 426:450–454. https://doi.org/10.1038/nature02145.
18. Letko M, Marzi A, Munster V. 2020. Functional assessment of cell entry and receptor usage for SARS-CoV-2 and other lineage B betacoronaviruses. Nat Microbiol 5:562–569. https://doi.org/10.1038/s41564-020-0688-y.
19. Hoffmann M, Kleine-Weber H, Schroeder S, Kruger N, Herrler T, Erichsen S, Schiergens TS, Herrler G, Wu NH, Nitsche A, Muller MA, Drosten C, Pohlmann S. 2020. SARS-CoV-2 cell entry depends on ACE2 and TMPRSS2 and is blocked by a clinically proven protease inhibitor. Cell 181:271–280. https://doi.org/10.1016/j.cell.2020.02.052.
20. Yan R, Zhang Y, Li Y, Xia L, Guo Y, Zhou Q. 2020. Structural basis for the recognition of the SARS-CoV-2 by full-length human ACE2. Science 367:1444–1448. https://doi.org/10.1126/science.abb2762.
21. Lan J, Ge J, Yu J, Shan S, Zhou H, Fan S, Zhang Q, Shi X, Wang Q, Zhang

L, Wang X. 2020. Structure of the SARS-CoV-2 spike receptor-binding domain bound to the ACE2 receptor. Nature 581:215–220. https://doi.org/10.1038/s41586-020-2180-5.
22. Li F, Li W, Farzan M, Harrison SC. 2005. Structure of SARS coronavirus spike receptor-binding domain complexed with receptor. Science 309:1864–1868. https://doi.org/10.1126/science.1116480.
23. Wrobel AG, Benton DJ, Xu P, Roustan C, Martin SR, Rosenthal PB, Skehel JJ, Gamblin SJ. 2020. SARS-CoV-2 and bat RaTG13 spike glycoprotein structures inform on virus evolution and furin-cleavage effects. Nat Struct Mol Biol 27:763–767. https://doi.org/10.1038/s41594-020-0468-7.
24. Walls AC, Park YJ, Tortorici MA, Wall A, McGuire AT, Veesler D. 2020. Structure, function, and antigenicity of the SARS-CoV-2 spike glycoprotein. Cell 181:281–292. https://doi.org/10.1016/j.cell.2020.02.058.
25. Wrapp D, Wang N, Corbett KS, Goldsmith JA, Hsieh CL, Abiona O, Graham BS, McLellan JS. 2020. Cryo-EM structure of the 2019-nCoV spike in the prefusion conformation. Science 367:1260–1263. https://doi.org/10.1126/science.abb2507.
26. Wong SK, Li W, Moore MJ, Choe H, Farzan M. 2004. A 193-amino acid fragment of the SARS coronavirus S protein efficiently binds angiotensin-converting enzyme 2. J Biol Chem 279:3197–3201. https://doi.org/10.1074/jbc.C300520200.
27. Moore MJ, Dorfman T, Li W, Wong SK, Li Y, Kuhn JH, Coderre J, Vasilieva N, Han Z, Greenough TC, Farzan M, Choe H. 2004. Retroviruses pseudotyped with the severe acute respiratory syndrome coronavirus spike protein efficiently infect cells expressing angiotensin-converting enzyme 2. J Virol 78:10628–10635. https://doi.org/10.1128/JVI.78.19.10628-10635.2004.
28. Shi J, Wen Z, Zhong G, Yang H, Wang C, Huang B, Liu R, He X, Shuai L, Sun Z, Zhao Y, Liu P, Liang L, Cui P, Wang J, Zhang X, Guan Y, Tan W, Wu G, Chen H, Bu Z. 2020. Susceptibility of ferrets, cats, dogs, and other domesticated animals to SARS-coronavirus 2. Science 368:1016–1020. https://doi.org/10.1126/science.abb7015.
29. Zhang Q, Zhang H, Huang K, Yang Y, Hui X, Gao J, He X, Li C, Gong W, Zhang Y, Peng C, Gao X, Chen H, Zou Z, Shi Z, Jin M. 2020. SARS-CoV-2 neutralizing serum antibodies in cats: a serological investigation. bioRxiv https://doi.org/10.1101/2020.04.01.021196.
30. Enserink M. 2020. Coronavirus rips through Dutch mink farms, triggering culls. Science 368:1169. https://doi.org/10.1126/science.368.6496.1169.
31. Oreshkova N, Molenaar RJ, Vreman S, Harders F, Oude Munnink BB, Hakze-van der Honing RW, Gerhards N, Tolsma P, Bouwstra R, Sikkema RS, Tacken MG, de Rooij MM, Weesendorp E, Engelsma MY, Bruschke CJ, Smit LA, Koopmans M, van der Poel WH, Stegeman A. 2020. SARS-CoV-2 infection in farmed minks, the Netherlands, April and May 2020. Euro Surveill 25:2001005. https://doi.org/10.2807/1560-7917.ES.2020.25.23.2001005.
32. Wang M, Cregeen S, Ajami N, Petrosino J. 2020. Evidence of recombination in coronaviruses implicating pangolin origins of nCoV-2019. bioRxiv https://doi.org/10.1101/2020.02.07.939207.
33. Kruse R. 2020. Therapeutic strategies in an outbreak scenario to treat the novel coronavirus originating in Wuhan, China. F1000Res 9:72. https://doi.org/10.12688/f1000research.22211.2.
34. Lui I, Zhou XX, Lim SA, Elledge SK, Solomon P, Kettko NJ, Zha BS, Kirkemo LL, Gramespacher JA, Liu J, Muecksch F, Lorenzi JCC, Schumidt F, Weisblum Y, Robbiani DF, Nussenzweig MC, Hatziioannou T, Bieniasz P, Rosenburg OS, Leung KK, Wells JA. 2020. Trimeric SARS-CoV-2 Spike interacts with dimeric ACE2 with limited intra-Spike avidity. bioRxiv https://doi.org/10.1101/2020.05.21.109157.
35. Case JB, Rothlauf PW, Chen RE, Liu Z, Zhao H, Kim AS, Bloyet L-M, Zeng Q, Tahan S, Droit L, Ilagan MXG, Tartell MA, Amarasinghe G, Henderson JP, Miersch S, Ustav M, Sidhu S, Virgin HW, Wang D, Ding S, Corti D, Theel ES, Fremont DH, Diamond MS, Whelan SPJ. 2020. Neutralizing antibody and soluble ACE2 inhibition of a replication-competent VSV-SARS-CoV-2 and a clinical isolate of SARS-CoV-2. bioRxiv https://doi.org/10.1101/2020.05.18.102038.
36. Monteil V, Kwon H, Prado P, Hagelkruys A, Wimmer RA, Stahl M, Leopoldi A, Garreta E, Hurtado Del Pozo C, Prosper F, Romero JP, Wirnsberger G, Zhang H, Slutsky AS, Conder R, Montserrat N, Mirazimi A, Penninger JM. 2020. Inhibition of SARS-CoV-2 infections in engineered human tissues using clinical-grade soluble human ACE2. Cell 181:905–913. https://doi.org/10.1016/j.cell.2020.04.004.
37. Strohl WR. 2015. Fusion proteins for half-life extension of biologics as a strategy to make biobetters. BioDrugs 29:215–239. https://doi.org/10.1007/s40259-015-0133-6.
38. Liu P, Wysocki J, Souma T, Ye M, Ramirez V, Zhou B, Wilsbacher LD, Quaggin SE, Batlle D, Jin J. 2018. Novel ACE2-Fc chimeric fusion provides long-lasting hypertension control and organ protection in mouse models of systemic renin angiotensin system activation. Kidney Int 94:114–125. https://doi.org/10.1016/j.kint.2018.01.029.